AMERICAN SOCIETY FOR MICROBIOLOGY | Infection and Immunity®

FUNGAL AND PARASITIC INFECTIONS

Alteration of Fermentative Metabolism Enhances *Mucor circinelloides* Virulence

Sharel P. Díaz-Pérez,[a] J. Alberto Patiño-Medina,[a] Marco I. Valle-Maldonado,[a] Adolfo López-Torres,[b] Irvin E. Jácome-Galarza,[c] Verónica Anaya-Martínez,[d] Verónica Gómez-Ruiz,[e] Jesús Campos-García,[a] Rosa E. Nuñez-Anita,[f] Rafael Ortiz-Alvarado,[g] Martha I. Ramírez-Díaz,[a] J. Félix Gutiérrez-Corona,[h] Víctor Meza-Carmen[a]

[a]Instituto de Investigaciones Químico Biológicas, Universidad Michoacana de San Nicolás de Hidalgo (UMSNH), Morelia, Michoacán, México
[b]Universidad Papaloapan, Campus Tuxtepec, Tuxtepec, Oaxaca, México
[c]Departamento de Biología Molecular, Laboratorio Estatal de Salud Pública del Estado de Michoacán, Morelia, Michoacán, México
[d]Facultad de Ciencias de la Salud, Universidad Anáhuac, Huixquilucan, Estado de México, México
[e]Laboratorio de Patología, Hospital Civil "Dr. Miguel Silva," Morelia, Michoacán, México
[f]Facultad de Medicina Veterinaria y Zootecnia, Universidad Michoacana de San Nicolás Hidalgo, Morelia, Michoacán, México
[g]Facultad de Químico Farmacobiología, Universidad Michoacana de San Nicolás Hidalgo, Morelia, Michoacán, México
[h]Departamento de Biología, División de Ciencias Naturales y Exactas, Universidad de Guanajuato, Guanajuato, Guanajuato, México

J. Félix Gutiérrez-Corona and Víctor Meza-Carmen are co-senior authors.

ABSTRACT The fungus *Mucor circinelloides* undergoes yeast-mold dimorphism, a developmental process associated with its capability as a human opportunistic pathogen. Dimorphism is strongly influenced by carbon metabolism, and hence the type of metabolism likely affects fungus virulence. We investigated the role of ethanol metabolism in *M. circinelloides* virulence. A mutant in the *adh1* gene (M5 strain) exhibited higher virulence than the wild-type (R7B) and the complemented (M5/pEUKA-*adh1*$^+$) strains, which were nonvirulent when tested in a mouse infection model. Cell-free culture supernatant (SS) from the M5 mutant showed increased toxic effect on nematodes compared to that from R7B and M5/pEUKA-*adh1*$^+$ strains. The concentration of acetaldehyde excreted by strain M5 in the SS was higher than that from R7B, which correlated with the acute toxic effect on nematodes. Remarkably, strain M5 showed higher resistance to H_2O_2, resistance to phagocytosis, and invasiveness in mouse tissues and induced an enhanced systemic inflammatory response compared with R7B. The mice infected with strain M5 under disulfiram treatment exhibited only half the life expectancy of those infected with M5 alone, suggesting that acetaldehyde produced by *M. circinelloides* contributes to the toxic effect in mice. These results demonstrate that the failure in fermentative metabolism, in the step of the production of ethanol in *M. circinelloides*, contributes to its virulence, inducing a more severe tissue burden and inflammatory response in mice as a consequence of acetaldehyde overproduction.

KEYWORDS *Mucor circinelloides*, fermentative metabolism, alcohol dehydrogenase, acetaldehyde, ethanol, virulence, alcohol, mucoral, mucormycosis, oxidoreductases, dimorphism

Fungal infections are a major threat to immunosuppressed patients (1) and contribute significantly to nosocomial infections in critical care units (2). Fungal infections can be superficial or invasive, with invasive infections being a major cause of morbidity and mortality in patients with cancer and immunosuppression (3). Mucormycoses are among the fungal infections becoming the most common in the last decade, along with invasive aspergillosis, which is in part a consequence of improved laboratory diagnoses (4). Members of the genera *Rhizopus*, *Rhizomucor*, *Mucor*, and *Absidia* are the

Citation Díaz-Pérez SP, Patiño-Medina JA, Valle-Maldonado MI, López-Torres A, Jácome-Galarza IE, Anaya-Martínez V, Gómez-Ruiz V, Campos-García J, Nuñez-Anita RE, Ortiz-Alvarado R, Ramírez-Díaz MI, Gutiérrez-Corona JF, Meza-Carmen V. 2020. Alteration of fermentative metabolism enhances *Mucor circinelloides* virulence. Infect Immun 88:e00434-19. https://doi.org/10.1128/IAI.00434-19.

Editor Liise-anne Pirofski, Albert Einstein College of Medicine

Address correspondence to Víctor Meza-Carmen, victor_meza2004@yahoo.com.mx.

Received 6 June 2019
Returned for modification 11 July 2019
Accepted 22 October 2019
Accepted manuscript posted online 4 November 2019
Published 22 January 2020

most frequent etiological agents isolated from patients with mucormycosis (5), which yields an overall mortality of up to 90% when left untreated in susceptible populations (6). *Rhizopus* and *Mucor* species cause the majority of mucormycosis, with mortality rates of up to 50%, even in the presence of antifungal therapy (7). Neutropenia, elevated blood serum iron concentration, and malignancies represent risks associated with poor prognosis of mucormycosis (8).

Few virulence factors with well-known biochemical and molecular bases have been described in *Mucorales*. In *Mucor circinelloides*, the size of the spores, which is modulated by calcineurin, is a virulence factor, since mutations in the *cnaA* gene, encoding the calcineurin subunit A, cause the production of spores that are larger and more virulent than spores produced by the wild-type strain (9). Morphological transitions also contribute to virulence during host infection by *M. circinelloides*. Under aerobic conditions the wild-type strain develops abundant hyphae, whereas mutants in the *cnbR* gene, which encodes the *M. circinelloides* calcineurin regulatory subunit B, produced yeast cells and exhibited reduced virulence compared to the wild-type strain (9). Mutation of genes encoding ADP-ribosylation factor 1 (Arf 1) and Arf 3 and Arf-like (Arl) protein 1 led to the secretion of a harmful protein(s) that contributed to increasing the pathogenesis of *M. circinelloides* (10, 11). *Rhizopus oryzae* uses the GRP78 surface protein, which is overproduced during diabetic ketoacidosis, to cause endothelial cell invasion and damage in mice (12). Spores of *M. circinelloides* produced on medium supplemented with native blood serum are more resistant to H_2O_2 and macrophage phagocytosis and increase the virulence capacity compared to *M. circinelloides* spores produced on medium supplemented with denatured blood serum or on medium alone (13).

Other fungal pathogens utilize an extended repertoire of virulence factors, including toxins (aflatoxins produced by some *Aspergillus flavus* strains), hydrolases (lipases, proteases), and glycoproteins for host cell binding (14). In the most common human fungal pathogen, *Candida albicans*, the ability to form biofilms constitutes a major virulence factor (15). Two lines of study suggest a link between ethanol metabolism and biofilm formation. Ethanol inhibits biofilm development; moreover, genetic alteration of the alcohol dehydrogenase (Adh) enzyme increases the capacity of *C. albicans* to form biofilms in which the ethanol level is low but the level of acetaldehyde is high (16). In *Aspergillus fumigatus*, ethanol metabolism has been implicated in the adaptation to hypoxia conditions during mouse infection. The *alcC* gene from *A. fumigatus*, encoding an alcohol dehydrogenase, is highly expressed in the fungus infecting the lungs from immunosuppressed mice. Moreover, *alcC* mutation results in reduced fungal presence in tissues and increases the inflammatory response (17). In relation to *M. circinelloides*, biochemical and genetic evidence indicates that the ADH1 enzyme is responsible for ethanol production from acetaldehyde reduction and that *adh1* gene expression is greater in yeast cells than mycelial cells (18, 19). *M. circinelloides adh1* gene mutation prevents growth under anaerobic conditions and leads to decreased ethanol production and reduced capacity to grow in ethanol, confirming its role in fermentative and oxidative metabolism (20).

Because *Mucor* dimorphism and carbon metabolism are strongly linked (20, 21), we sought to determine the effects of ethanol metabolism on *M. circinelloides* virulence. To this end, we tested the effect of the *adh1*$^-$ mutation on the virulence as well as the inflammatory response in both mouse and nematode infection models.

RESULTS

***adh1* gene mutation increases *M. circinelloides* virulence.** *M. circinelloides* exhibits a dimorphic process, and the hyphal growth has been suggested to increase its virulence (9). Our group observed that the *M. circinelloides adh1* mutant (M5) is unable to grow under anaerobic conditions and shows diminished ethanol production (20). To determine the role of Adh1 in *M. circinelloides* virulence, we tested the effects of *adh1* mutation in a survival assay using normal nonimmunodepressed BALB/c mice and the nematode *Caenorhabditis elegans* as infection models.

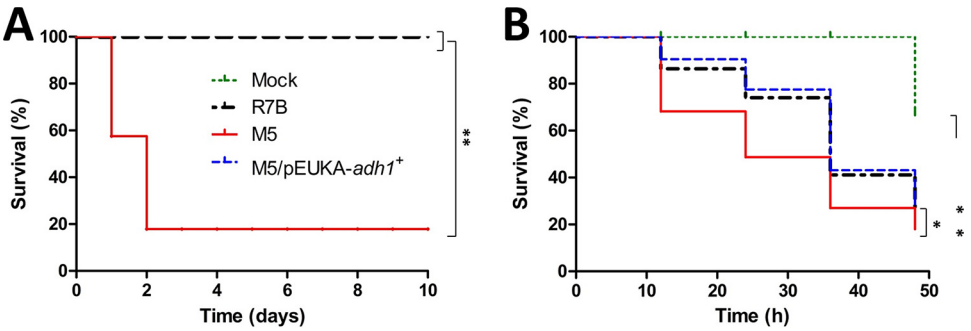

FIG 1 The *adh1*$^-$ mutation increases virulence in *M. circinelloides*. (A) A total of 5×10^6 spores from each of the different strains (M5, *adh1*$^-$ mutant; R7B, *adh1* wild type; M5/pEUKA-*adh1*$^+$, *adh1* mutant complemented) were inoculated using intraperitoneal administration in normal male BALB/c mice. Groups of 8 animals were treated with the different strains. The animals were observed daily until their death. (B) For *C. elegans* infection assays, 24-well flat-bottom plates were incubated with 10,000 spores and 20 nematodes per well in 1 ml of Lee medium; living nematodes were monitored every 12 h. Three independent experiments were registered in each host model of infection. The data were statistically analyzed using the Kaplan-Meier test. *, $P < 0.05$; **, $P < 0.01$; ***, $P < 0.001$. When results were not considered significant, we did not provide an additional indication ($P < 0.1$).

Intraperitoneal injection of spores from wild-type (R7B), *adh1*$^-$ (M5), and complemented M5 mutant (M5/pEUKA-*adh1*$^+$) strains clearly showed that M5 dramatically increased *M. circinelloides* virulence compared to R7B or M5/pEUKA-*adh1*$^+$. Strain M5 administration resulted in 82.14% lethality 2 days postinoculation, whereas all mice inoculated with spores from R7B or M5/pEUKA-*adh1*$^+$ survived throughout all assayed periods (Fig. 1A). In correlation, nematode inoculation with spores from strain M5 led to a significant increase in virulence compared to R7B or the M5/pEUKA-*adh1*$^+$ spores (Fig. 1B). This result indicated that the *adh1* mutation leads to increased fungal virulence.

Mutation of *adh1* affects *M. circinelloides* germination and growth during aerobic development. It has been reported that an increase in germination correlates with a higher virulence rate in *M. circinelloides* (11). Thus, we next addressed whether enhanced strain M5 virulence is due to an increase in the germination and/or growth rate. Strain M5 exhibited a significantly lower germination rate (Fig. 2A) and diminished biomass production (growth) in minimal medium (Fig. 2B) compared to strains R7B and M5/pEUKA-*adh1*$^+$. These results indicated that virulence enhancement in M5 did not correlate with an increase of germination or growth rate in the strain. Assessment of hyphal morphology in mycelia growing under aerobic conditions did not reveal any significant morphological change in the M5 mutant compared to the wild-type R7B

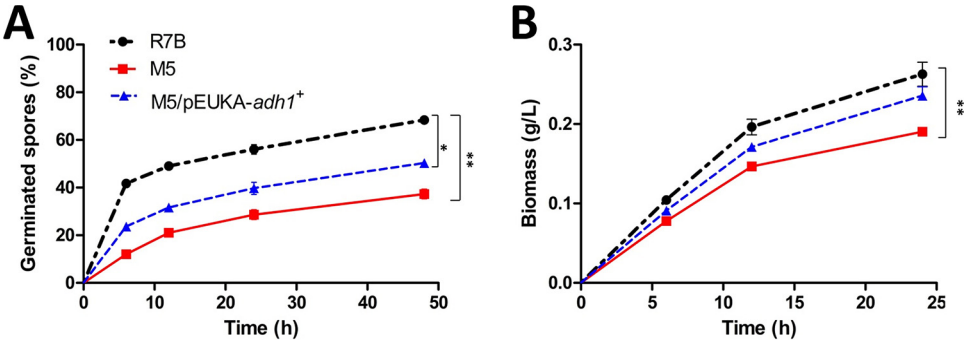

FIG 2 The aerobic development of *M. circinelloides* is affected by mutation of the *adh1* gene. A total of 5×10^5 spores per ml were inoculated into minimal (Lee) liquid medium supplemented with leucine at 28°C with constant shaking. The germination rate (A) and growth (B) were registered at the indicated times for the three strains (M5, *adh1*$^-$ mutant; R7B, *adh1* wild type; M5/pEUKA-*adh1*$^+$, *adh1* mutant complemented). Four independent experiments were performed under the same conditions. Significance testing was performed using the unpaired Student's *t* test. *, $P < 0.05$; **, $P < 0.01$; ***, $P < 0.001$. When results were not considered significant, we did not provide an additional indication ($P < 0.1$).

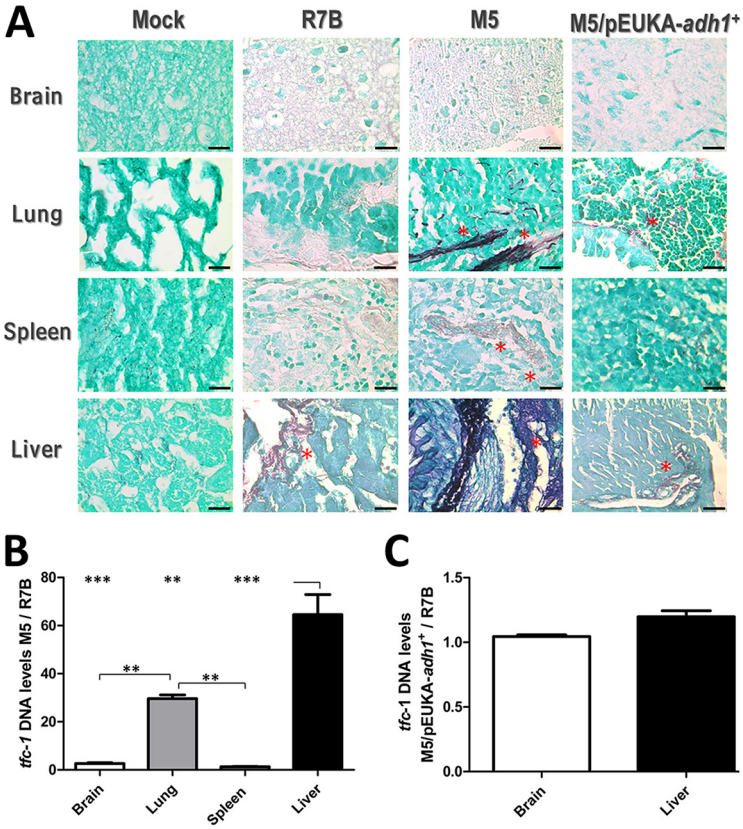

FIG 3 Mutation in the *adh1* gene increases the invasiveness of *M. circinelloides*. A total of 5×10^6 spores from each of the different strains of *M. circinelloides* (M5, *adh1*$^-$ mutant; R7B, *adh1* wild type; M5/pEUKA-*adh1*$^+$, *adh1* mutant complemented with *adh1* wild type [WT]) were inoculated independently per mouse. Following 48 h of incubation, animals were sacrificed and the organs were removed to be observed (A). Asterisks indicate the presence of *M. circinelloides* hyphae in tissues subjected to Grocott staining. Images were taken with ×100 magnification under light microscopy. Bar = 200 μm. (B) Quantification of fungal load in the different mouse tissues by qPCR using *tfc-1* from *M. circinelloides*. The values shown in the ordinate of the graph correspond to the ratio of the *tfc-1* gene signal detected in the tissues by treatment with strain M5 or R7B. (C) We also analyzed the ratio of the *tfc-1* gene from the tissues infected with M5/pEUKA-*adh1* or R7B. Mouse β-actin gene was used to validate the use of the same amount of DNA from the different mouse tissues. Four independent experiments were performed under the same conditions. Significance testing was performed using the unpaired Student's *t* test. *, $P < 0.05$; **, $P < 0.01$; ***, $P < 0.001$. When results were not considered significant, we did not provide an additional indication ($P < 0.1$).

strain (see Fig. S1 in the supplemental material). *M. circinelloides* spore size has been associated with virulence changes, with a larger spore size correlating with higher virulence (22). However, spore size determination by flow cytometry and optical microscopy showed that all three strains produced spores of equivalent size (Fig. S2).

Mutation of *adh1* enhances mouse organ invasion by *M. circinelloides*. Fungal cells' infectivity largely depends on their capability of deep tissue invasion (23), that is, being able to penetrate organs such as the lung, liver, spleen, and brain. The different *M. circinelloides* strains were intraperitoneally inoculated to simulate acute sepsis in the murine model, and all animals were sacrificed and the organs removed prior to natural death. Fungal tissue invasion and burden were determined qualitatively with Grocott staining of the tissue sections and quantitatively with real-time quantitative PCR (qPCR) using the *M. circinelloides tfc-1* gene (19). In general, the histological analysis revealed that in all tissues studied, the presence of the fungus (dark color) was more evident in the mouse tissues infected with strain M5 (Fig. 3A). Following infection with strain M5, the organ with the highest signs of fungal burden was the liver, followed by the lungs, whereas the brain and spleen demonstrated lower fungal presence (Fig. 3A). Using the same amount of mouse genomic DNA isolated from the tissues of mice infected with

the different *M. circinelloides* strains, fungal DNA was quantified using qPCR analysis (Fig. S3), and the results obtained were consistent with the cytology, indicating that after infection with M5, the liver and lungs from mice displayed ~80-fold higher fungal load than that following R7B infection (Fig. 3B). M5 also yielded higher fungal content in the brain and spleen, although this proportion was no more than 5-fold higher than that of R7B. In general, these findings indicated that M5 has a higher capacity to invade and colonize tissues than strains R7B and M5/pEUKA-*adh1*$^+$, which did not markedly differ in their capacity (Fig. 3C).

Trying to explain the increased capability of strain M5 to invade tissues, we evaluated the capability of *M. circinelloides* strains to survive under oxidative stress, determining the ability of the spores to germinate on yeast-peptone-glucose (YPG) medium after the addition of H_2O_2. The spores from strain M5 showed the highest levels of resistance to H_2O_2, with ~64% of spores germinated, strain M5/pEUKA-*adh1*$^+$ showed ~54% of spores germinated, and the spores from the wild-type strain showed ~37% germination compared to the control without H_2O_2 (Fig. 4A). After obtaining this result, we performed a phagocytosis assay with the spores from all the strains using the murine macrophage cell line RAW 264.7. We observed spore germination in the presence of the macrophages after 3 h of interaction, and spores from strain M5 seemed to germinate faster than those from the other strains (Fig. 4B). To quantify the spore germination, mRNA of *pkaR1* was used to indirectly estimate the aerobic spore germination (19). The mRNA levels of *pkaR1* were determined by real-time quantitative reverse transcription-PCR (qRT-PCR) after 1, 3, or 6 h of macrophage and spore interaction. The *pkaR1* transcript levels after 1 h (~264 or ~118%), 3 h (~143 or ~42%), and 6 h (~122 or ~36%) were higher in the M5 strain than the wild-type or M5/pEUKA-*adh1*$^+$ strain (Fig. 4C). We quantified the number of spores that were digested by macrophages after the interaction by qPCR using the *tfc-1* gene levels (see Materials and Methods). Our results showed that the lowest number of spores digested by the macrophages after 6 h of interaction corresponded to strain M5 (94,054 spores digested), followed by strain M5/pEUKA-*adh1*$^+$ (with 151,444 spores digested) and the wild-type strain (160,000 spores digested); this means that the spores digested in the mutant M5 correspond to only 60% and 65% of the spores digested in the wild-type and M5/pEUKA-*adh1*$^+$ strains, respectively (Fig. 4D). Additionally, we quantified the CFU produced from spores that survive the digestion by the macrophage after 6 h of interaction. Spores from the mutant M5 strain produced 36.6 or 42.6% more CFU after the macrophage interaction than the wild-type or M5/pEUKA-*adh1*$^+$ strain, respectively (Fig. 4E). These results indicate that the spores from the M5 mutant strain are less susceptible to digestion by the macrophages than the spores from the wild-type or M5/pEUKA-*adh1*$^+$ strain. Thus, these observations demonstrated that the genetic alteration of *M. circinelloides* fermentative metabolism by loss of function of the ADH1 enzyme increased the survival of spores after oxidative stress exposure and caused in the spores a greater resistance to the digestion by macrophages, which could explain in part the increased ability to invade and colonize tissues.

The *M. circinelloides adh1* gene mutation enhances the inflammatory response in mouse tissues. As the invasion of mouse tissues by *M. circinelloides* could trigger some response in the animal, it was of interest to determine whether there were changes in the inflammatory response as a result of the presence of the fungus and if such changes were differential between the M5, R7B, and complemented mutant (M5/pEUKA-*adh1*$^+$) strains of *M. circinelloides*. We utilized hematoxylin and eosin staining to analyze the morphological changes occurring in mouse tissues after infection with the various strains. Animals that had not been infected showed normal tissue appearance (Fig. 5A), whereas infection with the R7B or M5/pEUKA-*adh1*$^+$ strain caused mild inflammatory response in almost all tissues compared to tissues from noninfected animals (Fig. 5A). However, the tissues from mice infected with strain M5 showed more pronounced inflammation in brain and lungs. In the latter case, the alveolar structures were disrupted and erythrocytes were observed in the lung tissue, suggesting severe tissue damage. In addition, in mice infected with M5, the liver showed infiltration of

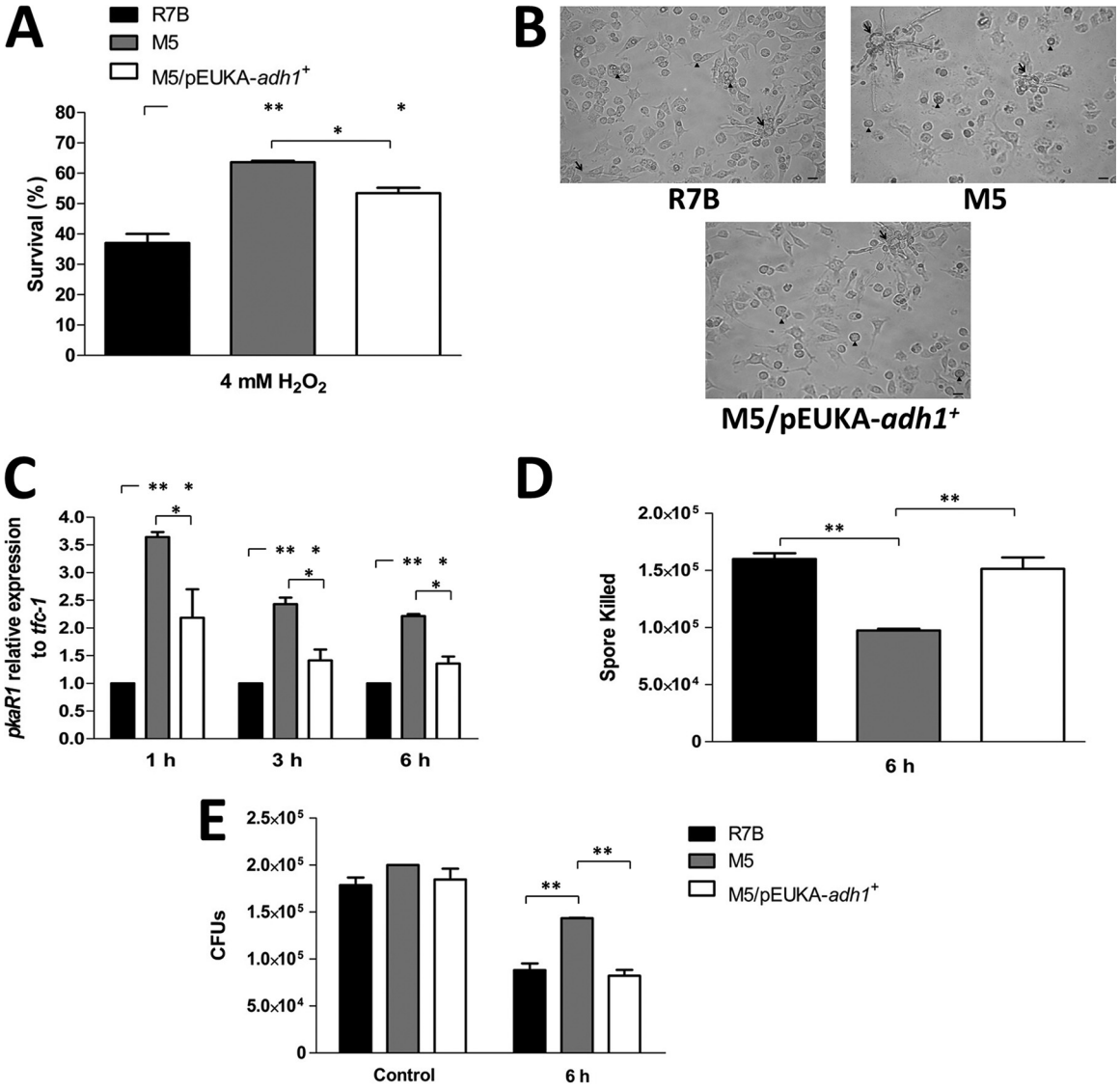

FIG 4 Role of the *adh1* mutation in the survival of *M. circinelloides* spores after H_2O_2 damage or macrophage phagocytosis. (A) Spores produced on YPG from the different strains were incubated with or without 4 mM H_2O_2 and incubated at 28°C. The survival rate was obtained after 24 h from the quotient of colonies from treatment versus no-treatment groups. (B) Germination of spores in the interaction with macrophages was seen under direct observation by light microscopy (×40). Scale bar = 20 μm. Arrows indicate germinating hyphae, and arrowheads indicate swelling spores. (C) The *pkaR1* mRNA levels were quantified using qRT-PCR 1, 3, and 6 h after the spores and macrophages interacted. (D) Quantitation of killed spores by qPCR using *tfc-1* after 6 h of incubation with mouse macrophages. A Δ*CT* analysis was performed to compare the mRNA and gene levels between the samples. (E) Quantitation of CFU from spores after 6 h of incubation with mouse macrophages. Figures show the average of three independent experiments. Significance testing was performed using the unpaired Student's *t* test. *, $P < 0.05$; **, $P < 0.01$; ***, $P < 0.001$. When results were not considered significant, we did not provide an additional indication ($P < 0.1$).

Kupfer cells and production of binucleated hepatocytes, indicating a more exacerbated inflammatory response than that seen in the tissue from animals infected with strains bearing functional ADH1 activity (Fig. 5A).

qRT-PCR analysis of some inflammatory responses (*Mip2*, *Il-1β*, and *Il-6*) in mice infected with *M. circinelloides* strains confirmed the observations made using histological analysis. The mice that were infected with strain M5 showed significantly higher transcript levels of these inflammation markers than did those infected with strains retaining functional ADH1 activity (Fig. 5B to D). Upregulated transcriptional activity of *Il-1β* and *Il-6* correlated with significantly elevated protein expression of interleukin 1β (IL-1β) and IL-6 in mouse liver and lung tissues that were previously infected with the mutant M5 strain (Fig. 6). These results indicate that the *adh1* mutation in *M. circinel-*

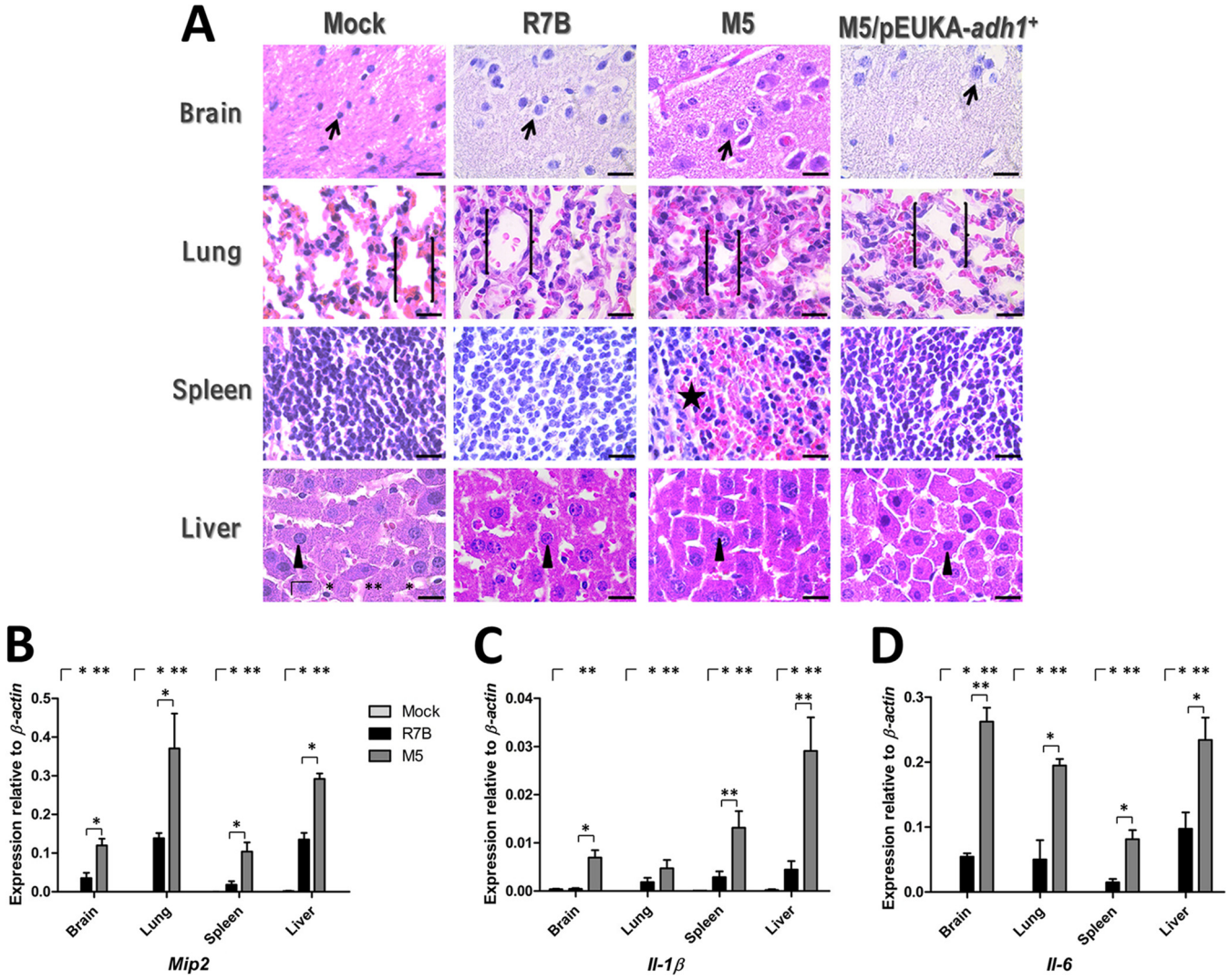

FIG 5 The *adh1*$^-$ mutant strain M5 of *M. circinelloides* triggers an enhanced inflammation response in mice. Spores from the different strains of *M. circinelloides* were inoculated in mice, and 48 h postinfection, the animals were sacrificed and the organs were removed for histological analysis using hematoxylin and eosin (A). The arrows show the glial brain cells. Alveolar structures are enclosed in brackets. The stars show the erythrocytes in the spleen, and the triangles show the hepatocyte morphology in the liver. Images were taken with ×100 magnification under light microscopy. Bar = 200 μm. mRNA quantification was performed in the organs, and levels of (B) *Mip2*, (C), *Il-1β*, and (D) *Il-6* were determined using qRT-PCR. Expression is relative to *Mus musculus* β-actin. Significance testing was performed using the unpaired Student's *t* test. *, $P < 0.05$; ** $P < 0.01$; ***, $P < 0.001$. When results were not considered significant, we did not provide an additional indication ($P < 0.1$).

loides induces a more pronounced systemic inflammatory response that could contribute to the lethal effect in infected mice.

Toxic effect of cell-free supernatant from the *M. circinelloides adh1* mutant. To understand the basis of the enhanced tissue burden and inflammation conferred by the *adh1* mutation, we tested if toxicity is mediated by excreted or secreted products of strain M5. To this end, cell-free culture medium (SS) from the different strains was collected and assayed for its effects on *C. elegans* viability in incubation performed at 20°C. The SS from strain M5 grown for 12 h caused the most pronounced loss of viability in *C. elegans* compared to strains R7B and M5/pEUKA-*adh1*$^+$ (Fig. 7A). M5-derived SS preincubated at 37°C or 37°C with addition of protease (pronase E) prior to nematode incubation similarly abolished the toxic effects on nematode viability (Fig. 7B and C). Moreover, the SS from all three strains incubated for 12 h at 25°C did not trigger any toxic effect on the nematode (Fig. 7D). Taken together, these results indicate that the M5 SS toxic effect is due to a thermolabile molecule of a nonprotein nature.

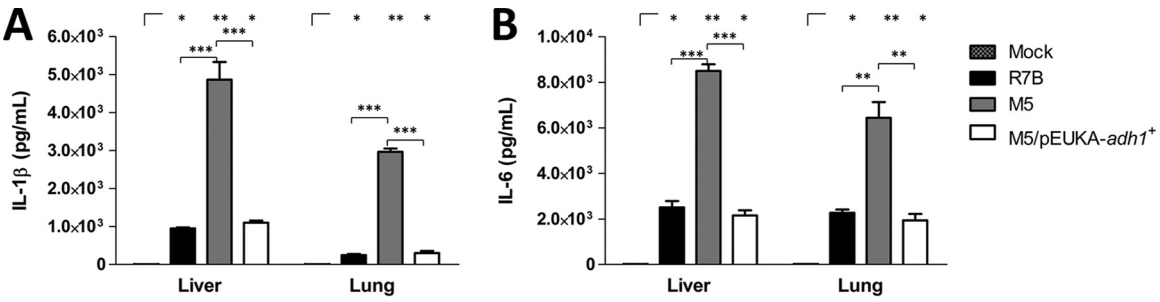

FIG 6 The *adh1*$^-$ mutant strain M5 of *M. circinelloides* increased the protein expression of cytokines in mouse tissue. The cytokine expression of (A) IL-1β and (B) IL-6 was determined using ELISA in liver and lung from mice previously infected for 48 h with the different strains. Significance testing was performed using the unpaired Student's *t* test. *, $P < 0.05$; **, $P < 0.01$; ***, $P < 0.001$. When results were not considered significant, we did not provide an additional indication ($P < 0.1$).

Toxic effect of the *M. circinelloides adh1* mutant is associated with excreted acetaldehyde. Because the toxic secreted compounds from strain M5 are temperature labile at 25°C as well as 37°C and because the *adh1* mutation impairs the synthesis of ethanol from acetaldehyde (20), we reasoned that among the possible compounds excreted in the culture medium of this strain, acetaldehyde best matches the characteristic of evaporation (acetaldehyde evaporates at 21°C). Strikingly, the SS acetaldehyde concentrations for strains R7B and M5/pEUKA-*adh1*$^+$ were 0.5 and 15 mM, respectively, whereas that of the M5 mutant strain was 47.5 mM (Fig. 8A). The SS from the M5 mutant strain was incubated for 12 h at 25°C or 37°C to promote the possible evaporation of acetaldehyde, and the concentration of acetaldehyde in the SS from strain M5 showed significantly reduced levels after incubation at 25°C (18 mM) and 37°C

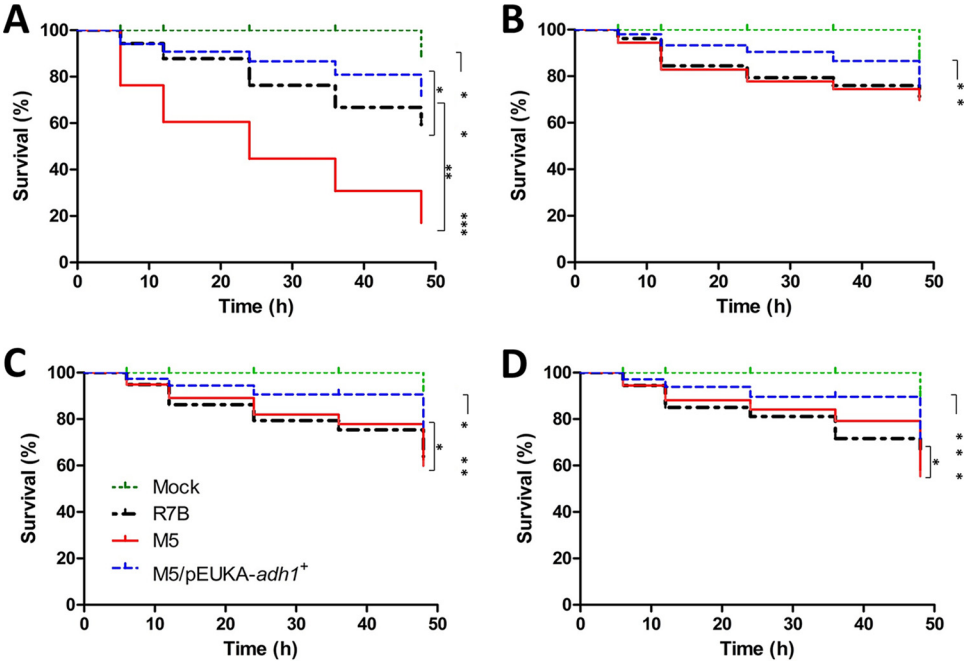

FIG 7 Cell-free medium from cultures of the *adh1*$^-$ mutant strain M5 of *M. circinelloides* is toxic to *Caenorhabditis elegans*. (A) Spores from the indicated strains were inoculated in Lee medium and grown under aerobic conditions at 28°C with constant shaking for 12 h, and then the cultures were filtered using 2-μm Millipore filters to obtain the cell-free medium culture (SS), which then was incubated in the presence of *C. elegans*. (B) The SS from all the strains were treated for 2 h at 37°C with pronase E or (C) at 37°C prior to incubation with the nematode. (D) The SS from all the strains were treated for 12 h at 25°C. All the SS were incubated with the nematodes. A total of 20 nematodes were used per well and incubated at 20°C for 2 h. The results presented are the average of four independent experiments. The data were statistically analyzed using the Kaplan-Meier test. *, $P < 0.05$; **, $P < 0.01$; ***, $P < 0.001$. When results were not considered significant, we did not provide an additional indication ($P < 0.1$).

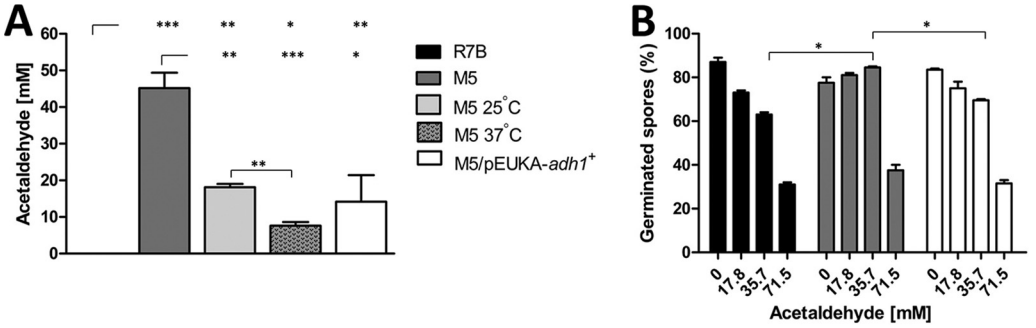

FIG 8 Acetaldehyde accumulation and its toxic effect during spore germination in *M. circinelloides adh1*$^-$ and *adh1*$^+$ strains. (A) The acetaldehyde from cell-free medium culture (from 12 h of fungal growth) was quantified using a mass spectrometry/flame ionization detector (MS-FID) method from different strains of *M. circinelloides* (M5, *adh1*$^-$ mutant; R7B, *adh1* wild type; M5/pEUKA-*adh1*$^+$, *adh1* mutant complemented). M5 cell-free medium culture was untreated (M5) or treated for 12 h at 25°C (M5 25°C) or at 37°C (M5 37°C). (B) Spore germination in the presence of exogenous addition of acetaldehyde in the various culture media. Four independent experiments were performed employing the same conditions. Significance testing was performed using the unpaired Student's *t* test. *, $P < 0.05$; **, $P < 0.01$; ***, $P < 0.001$. When results were not considered significant, we did not provide an additional indication ($P < 0.1$).

(7 mM) (Fig. 8A). Further experiments showed that the exogenous addition of acetaldehyde to *C. elegans* at a concentration of 37.5 mM led to a 60% viability loss (Fig. S4), indicating that this acetaldehyde concentration is toxic to *C. elegans* and explaining the high toxicity of M5 SS. Notably, acetaldehyde at 37.5 mM did not affect the spore germination rate of strain M5 at 6 h, although a 30% decrease of R7B spore germination was observed (Fig. 8B). This result indicates that strain M5 is uniquely able to cope with this acetaldehyde concentration, perhaps through its conversion to acetate.

In *Saccharomyces cerevisiae*, the *ald2*-encoded aldehyde dehydrogenase catalyzes the conversion of acetaldehyde to acetate (20). *ald2* mRNA quantitation from *M. circinelloides* strains showed that the *ald2* transcript level of R7B was 13.69-fold lower than that of strain M5 (Fig. 9A); moreover, the accumulation of acetate was 3.6-fold higher in strain M5 than strain R7B (Fig. 9B). These results suggest that the high accumulation of acetaldehyde in the M5 mutant strain activates a detoxification mechanism involving increased expression of the *ald2* gene, resulting in a greater tolerance to acetaldehyde in this strain.

Increased acetaldehyde production in the M5 *adh1* gene mutant strain contributes to its virulence in mice. In mammalian cells, acetaldehyde is metabolized to acetate by aldehyde dehydrogenase (ALD) activity; accordingly, when disulfiram, a competitive inhibitor of ALD activity, is used to control alcohol addiction, the resulting unpleasant symptoms and toxicity are due to acetaldehyde accumulation (24).

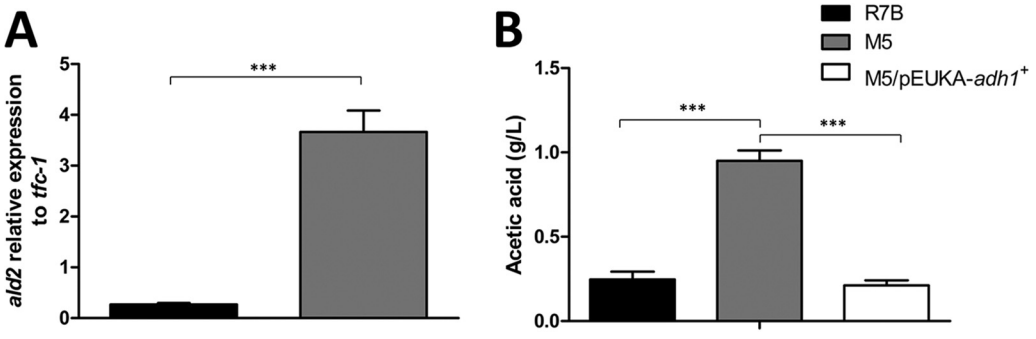

FIG 9 The *adh1*$^-$ mutant M5 from *M. circinelloides* detoxifies acetaldehyde through acetaldehyde dehydrogenase (*ald2*) overexpression. (A) Quantitation of the transcript levels of the acetaldehyde dehydrogenase gene (*ald2*) from wild-type (R7B) and *adh1*$^-$ mutant (M5) at 12 h of fungal growth. (B) Acetic acid levels were measured in the cell-free culture medium at 12 h of growth. Four independent experiments were performed under the same conditions. Significance testing was performed using the unpaired Student's *t* test. *, $P < 0.05$; **, $P < 0.01$; ***, $P < 0.001$. When results were not considered significant, we did not provide an additional indication ($P < 0.1$).

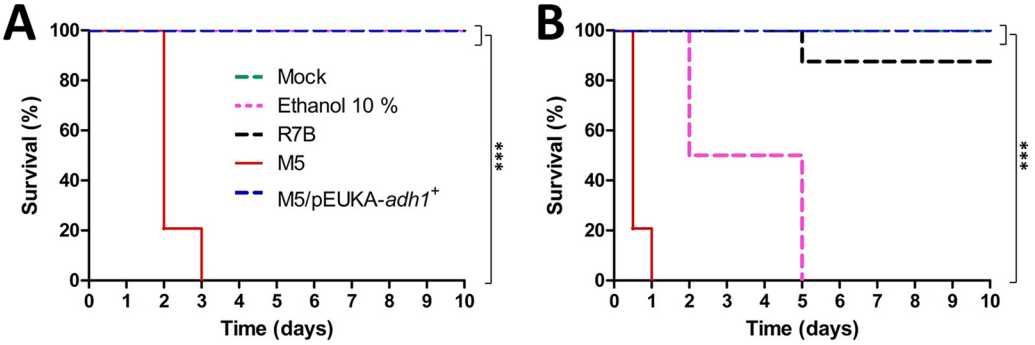

FIG 10 Mouse ALD activity inhibition increases the virulence of the *adh1*$^-$ mutant M5 of *M. circinelloides*. Spores from the different strains of *M. circinelloides* were inoculated independently per mouse. Mice were separated into two groups, which were not treated (A) or treated (B) with disulfiram and inoculated with spores from the *M. circinelloides* strains (M5, *adh1*$^-$ mutant; R7B, *adh1* wild type; M5/pEUKA-*adh1*$^+$, *adh1* mutant complemented). A positive control was used (mice with disulfiram treatment under the presence of ethanol at 10% *ad libitum*). Two independent experiments were performed employing the same conditions using 8 mice under each condition tested. The data were statistically analyzed using the Kaplan-Meier test. *, $P < 0.05$; **, $P < 0.01$; ***, $P < 0.001$. When results were not considered significant, we did not provide an additional indication ($P < 0.1$).

In the present study, disulfiram treatment was used in mice infected with the different strains of *M. circinelloides*, with treatment 48 h prior to spore infection and every 48 h postinfection. The administration of ethanol *ad libitum* did not generate mouse deaths (Fig. 10A), in contrast to the death of all mice at day 5 when ethanol was administered under disulfiram treatment (Fig. 10B). Remarkably, disulfiram treatment increased the virulence of strain M5, as shown by a decreased time until lethality compared to the result for mice that were infected with M5 alone (Fig. 10). In addition, 10% of the mice infected with R7B under disulfiram treatment were killed, in contrast to the 100% survival of mice infected with R7B spores without disulfiram treatment, suggesting that although much lower acetaldehyde is produced by mycelium from the wild-type R7B strain than strain M5 (Fig. 8A), it could be accumulated by the inhibitory effect of disulfiram on the ALD activity in strain R7B. This result suggests that the acetaldehyde accumulation, resulting from the inhibition of mouse ALD activity, enhanced the virulence effect of *M. circinelloides* strain M5.

DISCUSSION

Several zygomycetous species belonging to the order *Mucorales* function as human fungal pathogens to cause the lethal infection mucormycosis; these species include *Mucor* spp., *Rhizopus* spp., *Rhizomucor* spp., *Cunninghamella* spp., and *Apophysomyces trapeziformis* (25–27). In dimorphic species of *Mucor*, spore germination can lead to either filamentous (mycelium) or spherical (yeast) cell production, depending on environmental conditions (28, 29). The hyphal or the yeast phase of development can be obtained both in the presence of oxygen and under anaerobic conditions, depending on the carbon source and/or the presence of morphogenetic compounds. Development of the yeast form requires hexoses and invariably correlates with fermentative metabolism, whereas the hyphal phase can exhibit either oxidative or fermentative metabolism, depending on culture conditions (30). However, the type of metabolism is not a mandatory requirement for any of the *Mucor* dimorphism alternatives. Thus, as a consequence of altered *Mucor rouxii* fermentative metabolism by mutation of the *adh1* gene, the fungus loses its capacity to grow under anaerobic conditions. However, its spores maintain the ability to differentiate toward the yeast phase when incubated under aerobic conditions in the presence of phenethyl alcohol or to the hyphal phase upon incubation under aerobic conditions in medium without phenethyl alcohol (30). In *M. circinelloides*, the *adh1* gene is expressed in both hyphae and yeast cells, producing a cytoplasmic enzyme that appears to account for the major fungal ADH activity (18, 19). In addition, in *M. circinelloides* and *M. rouxii* the *adh1* gene mutation impairs growth under anaerobic conditions and negatively affects ethanol production

in aerobic cultures but does not affect the yeast-hypha dimorphism in aerobic conditions (20, 30). In recent years, specific signaling cascades, including the protein kinase A (31–34) and calcineurin pathways (9), have been implicated in the modulation of yeast-hyphal dimorphic transitions of *M. circinelloides*. Furthermore, it was shown that the pathogenicity of the fungus was negatively impacted upon calcineurin mutation (9).

In the present study, we show that alteration of the fermentative metabolism of *M. circinelloides* by *adh1* mutation exacerbates the pathogenic capacity of the fungus. In particular, the lack of ADH1 activity in the M5 mutant strain led to a higher mortality rate upon infection on mice or nematodes than that seen with the wild-type R7B and the complemented mutant M5/pEUKA-*adh1*$^+$ strains bearing functional ADH1 activity. Our previous kinetic studies showed that the *M. circinelloides* ADH1 enzyme possesses greater affinity for acetaldehyde than ethanol, revealing that *in vivo*, the main role of this enzyme is to convert acetaldehyde to ethanol (18). Our observations indicated that strain M5 produces higher acetaldehyde concentrations in the SS (45 mM) than do strains R7B (0.5 mM) and M5/pEUKA-*adh1*$^+$ (15 mM), lending further support to the fermentative function of the fungal ADH1 enzyme. This result also explains the higher toxic effects on *C. elegans* viability when exposed to SS from M5 than when exposed to SS from strains with functional ADH1 activity. Further observations supporting the model that the high concentration of acetaldehyde in the M5 SS accounts for the marked *C. elegans* loss of viability include (i) the decrease in the *M. circinelloides* strain-mediated SS toxicity effect by its incubation at 25°C and 37°C, which triggers acetaldehyde evaporation, and (ii) exogenous addition of acetaldehyde to *C. elegans* at a concentration similar to that produced by the M5 mutant, which recapitulates the M5 SS toxic effect in nematode viability. Notably, M5 overexpresses the *ald2* gene, which could be an acetaldehyde-induced response, as previously described in *S. cerevisiae* (35), aimed at acetaldehyde detoxification by its conversion to acetate.

Acetaldehyde is a highly toxic and carcinogenic product of alcohol fermentation and metabolism in microorganisms (36). In the dimorphic pathogen *C. albicans*, the ability to form biofilms constitutes a major virulence factor (37). Specifically, alcohol dehydrogenase is downregulated in *C. albicans* biofilms, and *ADH1* disruption significantly enhances the ability of the fungus to form biofilms in which the production of ethanol is low and that of acetaldehyde is high. Thus, it was concluded that ADH1 activity restricts the ability of *C. albicans* to form biofilms *in vitro* and *in vivo* and that the protein restricts biofilm formation through an ethanol-dependent mechanism (16). It was shown that in the presence of D,L-2-hydroxyisocaproic acid, *C. albicans* restricts biofilm formation and negatively affects the production of acetaldehyde from glucose; apparently, the latter process may be due to the upregulation of genes responsible for acetaldehyde catabolism (37, 38).

By using a chemotherapeutic murine model of invasive pulmonary aspergillosis and a metabolomics approach, ethanol was detected in the lungs of mice infected with *Aspergillus fumigatus*; it was demonstrated that during infection, the fungus is exposed to oxygen-depleted microenvironments (17). An Δ*alcC* mutant (which has the alcohol dehydrogenase-encoding gene *alcC* deleted) of *A. fumigatus* showed no growth defects under hypoxic conditions and yielded wild-type levels of mortality in different murine models. However, lung immunohistopathology and flow cytometry analyses revealed an increase in the inflammatory response in mice infected with the Δ*alcC* mutant strain, which corresponded to a reduction in fungal burden. It was concluded that in *A. fumigatus*, a functional ADH1 contributes to fungal pathogenesis in the lung, to hypoxia adaptation, and to growth (17).

The high degree of virulence of the *M. circinelloides* M5 *adh1* mutant in mice or in *C. elegans* demonstrates that altered fermentative metabolism, producing acetaldehyde accumulation, confers a greater capacity of pathogenesis and does not appear to negatively affect hypoxia adaptation during infection of mice, since the mutant M5 is not affected in its ability to colonize the host. In a previous study, we observed that the growth of the M5 mutant is drastically affected in *in vitro* cultures made under

anaerobic or in self-anaerobic conditions (20). Thus, the normal colonization of mice by the M5 mutant could indicate that nonfermentable carbon sources exist and could be used for growth in the environment of the animal's tissues and/or that hypoxia is not very strict in these tissues. Our findings reveal a mechanistic difference between *A. fumigatus* and *M. circinelloides* regarding the importance of the ADH1 enzyme in connection with pathogenic potential: in the former fungus, a functional ADH1 is required to sustain hypoxia adaptation and host colonization (18), whereas in *M. circinelloides*, the aforementioned enzymatic activity is not required for adaptation to hypoxia or for colonization of mice, and rather, the possession of a nonfunctional ADH1 increases the pathogenic potential of the fungus. Our results coincide in some aspects with those obtained in *C. albicans*, mainly with the observation that a decrease in ADH activity causes an increase in virulence. In *Candida*, this process is associated with an increase in biofilm formation, which constitutes a major virulence factor (37). In our observations, the mouse tissues (mainly liver and lungs) invaded by the M5 mutant showed fungal growth accumulation, but we were unable to determine if these hyphae were organized in biofilms. However, the fact that the SS from the three *M. circinelloides* strains studied were able to cause mortality in *C. elegans* indicated that hyphae are not the direct cause of damage to the nematode, but rather the acetaldehyde produced and excreted by strain M5 is the cause.

Wild-type *Candida* strains can produce acetaldehyde from ethanol or glucose in *in vitro* cultures (38). Our results show that in cultures grown in medium with glucose, the wild-type *M. circinelloides* strain R7B does not produce significant amounts of acetaldehyde. This may explain R7B's low degree of virulence compared to the M5 mutant strain, which produces acetaldehyde under these conditions, and indicates a metabolic difference between *Candida* and *Mucor*.

When cultured *in vitro* under aerobic conditions in the presence of glucose, the *M. circinelloides* M5 mutant showed a 35% decrease in germination rate and produced 33% less biomass than R7B. As *M. circinelloides* produces high levels of ethanol under aerobic conditions (18, 20), most likely such metabolism contributes to energy production, possibly through the regeneration of NAD^+, catalyzed by the ADH1 enzyme (18, 20). We propose that these detrimental effects could be the result of a lack of NAD^+ regeneration through the ADH1 activity in the M5 mutant strain. Unexpectedly, despite its reduced growth in cultures, the colonization of tissues by M5 was more extensive than that observed with strains R7B and M5/pEUKA-*adh1*$^+$. Probably, this is because strain M5 is more resistant to macrophage digestion in mice, as we observed in macrophage culture analysis.

In chronic lung inflammation in smokers (39) or heavy drinkers (40), acetaldehyde acts as a toxic compound that drives the inflammatory tissue response. The infection of mice with the Δ*alcC* mutant of *A. fumigatus* triggers an inflammatory response in their bronchoalveolar fluids (17). In the present study, we observed a similar effect in infections with the *M. circinelloides* M5 mutant, with an enhanced inflammatory response in all mouse tissues analyzed compared to that following R7B or M5/pEUKA-*adh1*$^+$ infection. We propose that overproduction of acetaldehyde contributes significantly to the M5 mutant's virulence and enhanced tissue burden in mice. Notably, 4.5 mM acetaldehyde inhibits phagocytosis and chemotaxis of monocytes and polymorphonuclear cells (41). This inhibitory effect may partially explain the enhanced tissue colonization by the M5 mutant strain compared to that of strains with functional ADH1 activity.

Our results indicated that the infection of mice with *M. circinelloides* M5 induced a systemic inflammatory response, even in brain tissue, suggesting a process of cell degranulation and blood histamine release. To test this assumption, we assessed the mRNA levels of three inflammatory response markers: (i) *Mip2*, whose mRNA expression is influenced by the presence of histamine (42), (ii) *Il-1β*, which is an important chemokine in the cell inflammatory response and apoptosis (43), and (iii) *Il-6*, the general response chemokine in inflammatory processes (44). These inflammatory response markers were expressed at a higher level of transcript (*Mip2*, *Il-1β*, and *Il-6*) and

protein (IL-1β and IL-6) in mouse tissues infected with the M5 mutant strain than those infected with *M. circinelloides* strains with functional ADH1 activity, indicating that strain M5 triggers a more pronounced inflammatory response.

In support of our model that acetaldehyde produced by *M. circinelloides* strain M5 is in part responsible for M5-associated pathology, treatment with the ALD inhibitor disulfiram, which increases acetaldehyde accumulation, exacerbated M5 virulence.

Acetaldehyde is produced by a conserved metabolic pathway in diverse human pathogens, including bacteria (*Enterobacteria* species), fungi (Ascomycetes: *C. albicans*, Zygomycetes: *Mucor* species), and protozoa (*Entamoeba* species); most of these organisms use fermentative metabolism during their infection process (45). To our knowledge, this is the first report that links ethanol metabolism and virulence in an early-diverging fungus. Furthermore, as *M. circinelloides* is a versatile fungus able to utilize diverse nutrients and oxygen concentrations to colonize its environment, it would be of considerable interest to identify a possible relationship between the prevalence and virulence of Mucorales strains (not only exclusive for *M. circinelloides*) from clinical origins and their characteristics in relation to ethanol metabolism.

MATERIALS AND METHODS

Strains and growth conditions. The *M. circinelloides* R7B (*leuA*$^-$) strain was originally derived from the (−) mating type *M. circinelloides* f. *lusitanicus* CBS 277.49 (46), M5 (*leuA*$^-$, *adh1*$^-$) is a spontaneous *adh1* mutant strain obtained by growth selection in allyl alcohol (20), and M5/pEUKA-*adh1*$^+$ is an M5 strain carrying a self-replicative plasmid (pEUKA-7) harboring the wild-type *adh1* gene from *M. circinelloides* R7B.

Spores were grown on yeast-peptone-glucose (YPG) medium containing 0.3% yeast extract, 1% gelatin peptone, and 2% glucose and supplemented as necessary with 2% bacteriological agar at pH 4.5. Minimum Lee medium was also employed, using 2% glucose, 0.5% sodium chloride, 0.25% potassium dihydrogen phosphate, 0.20% magnesium sulfate, 0.20% ammonium sulfate, 0.005% leucine as necessary, and 2% bacteriological agar supplemented when producing solid medium (adjusted pH 5.3).

Aerobic and self-anaerobic spore germination and growth quantification. Aerobic growth was performed in a 250-ml flask with 25 ml YPG inoculated with 5×10^5 *M. circinelloides* spores per ml. Liquid cultures were maintained at 28°C for 24 h with constant shaking at 150 rpm. Self-anaerobic spore germination was performed using 125-ml flasks with 125 ml YPG medium; 5×10^5 *M. circinelloides* spores per ml were incubated as described previously (47). The germination percentage was calculated for aerobic or anaerobic conditions as germinules or budding yeasts counted in a total of 100 cells. To determine biomass production, mycelia were collected from liquid cultures using filtration, and the dry weight was determined.

To evaluate the oxidative stress, 100 spores from each of the different strains were treated or not treated with 4 mM H_2O_2 for 1 h at 4°C and spread on YPG plates and incubated for 24 h at 28°C.

Total genomic DNA isolation from mouse tissues. DNA from mouse tissues infected or not infected with *M. circinelloides* strains was isolated as follows. Organs (brain, lung, spleen, and liver) were removed from the mouse postinoculation; tissue lysis was performed using 50 mg from each organ. Mouse tissue samples were transferred into a tube with MagNA Lyser green beads (Roche, Madison, WI, USA) and precooled on ice. Denaturing binding buffer (200 μl) and proteinase K (10 mg/ml, 40 μl) from the High Pure PCR template preparation kit (Roche) were added immediately before homogenization. For cell disruption, tubes were placed in the MagNA Lyser instrument (Roche) and processed twice at 4,200 $\times$ *g* for 40 s. Samples were cooled on ice for 1 min between each processing step. Samples were then centrifuged for 1 min at 15,000 $\times$ *g* (Eppendorf 5417), and the supernatants were used for DNA isolation following the manufacturer's protocol. Total genomic DNA was quantified using a Smart Spec Plus spectrophotometer (Bio-Rad, Berkeley, CA, USA).

Total RNA isolation from mouse tissues or *M. circinelloides*. Biological samples from the different *M. circinelloides* strains were collected 24 h after aerobic growth in YPG or Lee medium, filtered through Whatman filter paper (Sigma, St. Louis, MO, USA), and washed with distilled water. Mouse tissues (brain, lung, spleen, or liver) were also collected following *M. circinelloides* strain infection.

Approximately 50 mg of mycelia or mouse tissue samples was then transferred into a tube with MagNA Lyser green beads (Roche) precooled on ice. Denaturing RLT buffer (700 μl) from the RNeasy minikit (Qiagen, Venlo, The Netherlands) was added immediately before homogenization. For cell disruption, tubes were placed in the MagNA Lyser instrument and processed twice at 6,500 rpm for 40 s with cooling on ice for 1 min between each step. Then, samples were centrifuged for 1 min at 20,000 $\times$ *g* (Eppendorf 5417), and the supernatants were used for RNA isolation following the RNeasy minikit protocol (Qiagen). To eliminate DNA contamination, samples were treated with DNase I (Promega, Madison, WI, USA) according to the manufacturer's protocol. RNA samples were separated on nondenaturing 2% agarose gels stained with ethidium bromide, visualized using a Gel Doc XR+ imager (Bio-Rad, Hercules, CA, USA), and quantified using a SmartSpec Plus spectrophotometer (Bio-Rad).

Oligonucleotide design and real-time quantitative reverse transcription-PCR (qRT-PCR). Primers and hydrolysis probes for the *ald2* gene from *M. circinelloides* encoding the homolog to ALD2 from *Saccharomyces cerevisiae* were used as reported previously (20), and the β-actin (*Act*β), interleukin 1β

(*Il-1β*), interleukin 6 (*Il-6*), and murine macrophage inflammatory protein 2 (*Mip2*) genes from mice were used as described before (13).

qRT-PCR was performed using the LightCycler 480 II system (Roche Molecular Diagnostics, Pleasanton, CA, USA) employing the SuperScript III Platinum one-step qRT-PCR reagent kit (Invitrogen, Carlsbad, CA, USA). Each 25-μl reaction volume comprised 5 μl extracted total RNA template (50 ng), 0.5 μl enzyme mix, 12.5 μl reaction mix (2×), 0.5 μl each 10-μM forward and reverse primer, 0.5 μl probe (5 μM), and 5.5 μl nuclease-free water. qRT-PCR was initiated with reverse transcription (50°C, 30 min) and initial denaturation (95°C, 5 min), followed by 45 amplification cycles at 60°C for 30 s, 72°C for 30 s, and 95°C for 15 s; fluorescence signals were collected at each 60°C stage. Appropriate positive, nontemplate, and extraction controls were included in each test run.

Fungal load determination by real-time quantitative PCR from mouse tissues. The qPCR assay was performed using the LightCycler 480 II system with the Platinum quantitative PCR SuperMix-UDG kit (Invitrogen). Reactions were as above for qRT-PCR but with 5 μl extracted total DNA template (500 ng). qPCR was performed as indicated for qRT-PCR (without reverse transcriptase) and included the same controls as those employed for qRT-PCR; fluorescence signals were collected at each 60°C stage at 530 nm.

qRT-PCR and qPCR amplification efficiency, relative expression level calculation, and data analysis. To evaluate relative gene expression, a calculation for estimating the efficiency of a real-time PCR assay for each studied gene is required. Here, estimation was performed using a calibration dilution curve and slope calculation. A 5-fold dilution series (500 to 0.05 ng total RNA) was utilized as qRT-PCR samples. Briefly, E was obtained from standard curves using the formula $E = \{[10\ (-1/\text{slope}) - 1]/100\}$. Relative expression levels were determined using the efficiency correction method, considering amplification efficiencies between target and reference genes (48). *M. circinelloides tfc-1*, which encodes a subunit of the transcription factor TFIIIC required for the RNA polymerase III preinitiation complex assembly, served as the reference gene in qRT-PCR analysis during dimorphism in *M. circinelloides* (19).

***Caenorhabditis elegans* killing assays.** *C. elegans* Bristol N2 worms (49) were synchronized by hypochlorite isolation of eggs from gravid adults, followed by hatching in S-basal medium (50). L1 larvae were transferred onto nematode growth medium (50) plates seeded with the *Escherichia coli* OP50 strain previously grown on the plates as a food source and incubated at 20°C for 4 to 5 days until reaching young adult phase. Worms were rinsed from the plates and washed in S-basal medium. *M. circinelloides* cultures were grown at 12 or 24 h in YPG medium supplemented with leucine at 28°C and, after centrifugation, the SS was recovered by filtration (Millipore 0.2-μm filters; Billerica, MA, USA) for further experiments. For each experiment, 10 to 20 worms were dispensed into each well of 24-well Costar plates (Corning, Inc., Armonk, NY, USA). Then, worms were incubated with 1 ml SS or 10,000 spores from each strain contained in a total volume of 1 ml Lee medium, and the plates were incubated for 48 h at 20°C and scored for live worms at 6, 12, 24, and 48 h. For statistical purposes, three replicates per experiment were performed. YPG and Lee medium served as negative controls. A worm was considered dead when it no longer responded (moved) to a touch stimulus. Worms that died after sticking to the plate wall were excluded from the analysis.

For all assays, fungal inoculum concentrations were confirmed by dilution plating and counting. We conducted three independent assays for each worm group. The SS (1 ml) obtained from each *M. circinelloides* strain was treated with 25 μl pronase (Sigma), equivalent to 5 units, and incubated for 2 h at 37°C or heated at 90°C for 2 h prior to its use in the *C. elegans* killing assays.

Mouse virulence and disulfiram treatment. The protocol for the mouse virulence model followed the recommendations of the Mexican Federal Regulations for the Use and Care of Animals (NOM-062-ZOO-1999) (SAGARPA 2001) (51).

To assess *M. circinelloides* strain virulence, groups of approximately 10- to 12-week-old male BALB/c mice (CINVESTAV, Zacatenco, México) (20 g average weight) were used. At day 0, mice were inoculated with spores from the different *M. circinelloides* strains in 200 μl total volume of sterile phosphate-buffered saline containing 5×10^5 spores/dose administered intraperitoneally. Mouse survival was monitored each day. At least three independent assays were conducted for each group.

An ALD activity inhibitor (disulfiram; Sigma) was administered to the mice prior to and during the infection assay; each mouse was injected intraperitoneally with 300 mg/kg of body weight 48 h prior to spore inoculation and at day 0 of infection, followed by dosing each 48 h during the infection period. Mouse survival was monitored each 12 h after infection. Ethanol was administered by ingestion in drinking water at a concentration of 10% (vol/vol) supplied *ad libitum* to groups of male mice with or without disulfiram treatment.

Macrophage spore killing assay. Mouse monocyte/macrophage RAW 264.7 (TIB-71) was purchased from the American Type Culture Collection (ATCC). Cells were maintained in Dulbecco modified Eagle (DMEM) medium supplemented with 10% fetal bovine serum (FBS) (Sigma, USA), 100 U/ml penicillin (Sigma, USA), and 100 μg/ml streptomycin (Sigma, USA) (basal medium) at 5% CO_2 and 37°C 24 h before treatments.

Macrophages were seeded at 8×10^5 cells/well in DMEM basal medium (Gibco, Thermo Fisher Scientific, USA) without antibiotics and incubated at 37°C in 6-well plates. After incubation overnight, the basal medium in each well was replaced with fresh medium, and then the macrophages were cocultured with 2×10^5 spores produced in YPG for 1 or 6 h. Afterwards, the culture medium and cells and spores were separated by centrifugation at 1,000 × *g* for 10 min. The cell and spore pellet was recovered and resuspended in 0.1 ml and separated into two tubes with 0.05 ml each. One tube was maintained at −80°C until nucleic acid extraction was performed, and the other was diluted (1:50) and used to plate 200 of the initial spores to evaluate CFU in YPG solid medium. For the CFU assay, the control was the

spores in DMEM basal medium without antibiotics. The CFU were quantified 24 h after incubation in the presence of light at 28°C.

Preparation of tissue homogenate supernatants and ELISA. Spores from the different strains of *M. circinelloides* were inoculated intraperitoneally in BALB/c mice, and 48 h postinfection the animals were sacrificed and the organs were removed. Liver and lung organs were harvested, and the organs were transferred to a 2.0-ml microcentrifuge tube containing 0.8 ml phosphate-buffered saline (PBS) and protease inhibitor (cOmplete ultra tablets, mini, EDTA-free; Roche Diagnostics, Mannheim, Germany). The organs were homogenized by a Potter-Elvehjem glass homogenizer, and the supernatants were collected from the mixture following centrifugation at 10,000 × *g* for 10 min at 4°C and stored at −80°C prior to analysis. The protein expression level of IL-1β and IL-6 in the liver and lungs was determined using enzyme-linked immunosorbent assay (ELISA) following the manufacturer's instructions (Sigma, USA).

Determination of abundance of DNA from spores of *M. circinelloides* using qPCR. The abundance of spores of *M. circinelloides* from macrophage interaction was compared based on a spore standard curve of *M. circinelloides*. Wild-type R7B spore concentrations between 1×10^2 and 1×10^7 ml^{-1} by 10-fold serial dilutions were employed. Consequently, DNA was extracted to generate a spore standard curve by qPCR by detection of the validated *tfc-1* nuclear gene.

Histopathology. BALB/c mice were inoculated as described above and sacrificed at set time points after *M. circinelloides* inoculation. Organs were removed and fixed in 10% phosphate-buffered formalin, embedded in paraffin, sectioned at 5 μm, and stained with hematoxylin and eosin or Gomori methenamine silver using standard histological techniques. Microscopic examinations of the stained tissues were performed on a Leica M80/MSV266 instrument using a Leica DFC295 camera and the Leica Application Suite version 3.8.5 imaging system (Leica Microsystems Inc., Buffalo Grove, IL, USA).

Acetaldehyde and acetic acid quantitation. Acetaldehyde quantitation was performed using gas chromatography with a flame ionization detector on a 7890A series gas chromatograph (Agilent Technologies, Palo Alto, CA, USA) equipped with a WAX column (30 m length by 0.25 mm inside diameter [i.d.] by 0.25 μm film thickness) (Phenomenex, Torrance, CA, USA). Nitrogen was run as a carrier gas at a constant column flow rate of 0.7 ml/min. The temperature program was as follows: 40°C hold for 2 min, 5°C/min up to 60°C, 40°C up to 200°C for 0.5 min. The Split 20 injector was set at 200°C. Flame ionization detector temperatures were set at 250°C with H_2/airflow of 45/450 ml/210°C. Acetaldehyde was quantified using a calibration curve.

Acetic acid quantitation was performed as follows. Sodium hydroxide (NaOH) 0.05 N was prepared with cold water previously boiled for 3 min to eliminate dissolved CO_2; this NaOH solution was standardized with a 0.01 N HCl solution.

For preparation of each *M. circinelloides* supernatant sample, 100 ml previously boiled distilled water was added to a 250-ml Erlenmeyer flask, adjusted to pH 8.2 with 0.05 N NaOH solution and a Sartorius Professional PP-15 pH meter (Bohemia, NY, USA), and 5 ml supernatant was added. The solution was placed in a burette for titration to pH 8.2. The 0.05 N NaOH volume (in ml) necessary to neutralize the acid is directly proportional to the total acidity of acetic acid. The mathematical formula employed was:

$$\mathrm{TA\%} = 100\ (V_{\mathrm{titrate}} \times N_{\mathrm{titrate}} \times \text{citric acid Eqv. Wt.}) \cdot (V_S \times 100)$$

where TA is total acidity, $V_{titrate}$ is the volume of NaOH titrate employed, $N_{titrate}$ is the normality of the NaOH used in the reaction, citric acid Eqv. Wt. is 60.05, and V_s is the volume of sample. Using this approach, the quantity of total acetic acid produced was determined (g/liter).

Statistical analysis. Significance testing was performed using the unpaired Student's *t* test. *, $P < 0.05$; **, $P < 0.01$; ***, $P < 0.001$. When results were not considered significant, we did not provide an additional indication ($P < 0.1$).

SUPPLEMENTAL MATERIAL

Supplemental material is available online only.

SUPPLEMENTAL FILE 1, PDF file, 7.3 MB.

ACKNOWLEDGMENTS

We thank A.Y. Guzman-Hernandez for technical support in the initial mouse infection assays.

This work was supported by grants from Coordinación de la Investigación Científica (UMSNH; 2.6, 2.35) and Consejo Nacional de Ciencia y Tecnología (CONACYT; 181747, 167071). S.P.D.-P., J.A.P.-M., and M.I.V.-M. were supported by postgraduate fellowships from CONACYT.

S.P.D.-P., J.A.P.-M., M.I.V.-M., A.L.-T., I.E.J.-G., V.A.-M., V.G.-R., J.C.-G., R.E.N.-A., and R.O.-A. contributed to data acquisition, analysis, and data interpretation. J.C.-G., M.I.R.-D., J.F.G.-C., and V.M.-C. contributed to critical analysis, data interpretation, and critical revision of the article for intellectual content of the manuscript. J.F.G.-C. and V.M.-C. contributed to the conception and design of the work, data analysis, and interpretation. J.F.G.-C. and V.M.-C. wrote the majority of the article with minor contributions from the other authors.

We declare no conflicts of interest.

REFERENCES

1. Kim JY. 2016. Human fungal pathogens: why should we learn? J Microbiol 54:145–148. https://doi.org/10.1007/s12275-016-0647-8.
2. Matthaiou DK, Christodoulopoulou T, Dimopoulos G. 2015. How to treat fungal infections in ICU patients. BMC Infect Dis 15:205. https://doi.org/10.1186/s12879-015-0934-8.
3. Douglas AP, Chen SC, Slavin MA. 2016. Emerging infections caused by non-*Aspergillus* filamentous fungi. Clin Microbiol Infect 22:670–680. https://doi.org/10.1016/j.cmi.2016.01.011.
4. Pak J, Tucci VT, Vincent AL, Sandin RL, Greene JN. 2008. Mucormycosis in immunochallenged patients. J Emerg Trauma Shock 1:106–113. https://doi.org/10.4103/0974-2700.42203.
5. Petrikkos G, Skiada A, Lortholary O, Roilides E, Walsh TJ, Kontoyiannis DP. 2012. Epidemiology and clinical manifestations of mucormycosis. Clin Infect Dis 54:S23–S34. https://doi.org/10.1093/cid/cir866.
6. Neto FM, Camargo PC, Costa AN, Teixeira RH, Carraro RM, Afonso JE, Jr, Campos SV, Samano MN, Fernandes LM, Abdalla LG, Pêgo-Fernandes PM. 2014. Fungal infection by *Mucorales* order in lung transplantation: 4 case reports. Transplant Proc 46:1849–1851. https://doi.org/10.1016/j.transproceed.2014.05.033.
7. Cornely OA, Arikan-Akdagli S, Dannaoui E, Groll AH, Lagrou K, Chakrabarti A, Lanternier F, Pagano L, Skiada A, Akova M, Arendrup MC, Boekhout T, Chowdhary A, Cuenca-Estrella M, Freiberger T, Guinea J, Guarro J, de Hoog S, Hope W, Johnson E, Kathuria S, Lackner M, Lass-Flörl C, Lortholary O, Meis JF, Meletiadis J, Muñoz P, Richardson M, Roilides E, Tortorano AM, Ullmann AJ, van Diepeningen A, Verweij P, Petrikkos G, European Society of Clinical Microbiology and Infectious Diseases Fungal Infection Study Group, European Confederation of Medical Mycology. 2013. ESCMID and ECMM joint clinical guidelines for the diagnosis and management of mucormycosis. Clin Microbiol Infect 3:5–26. https://doi.org/10.1111/1469-0691.12371.
8. Binder U, Maurer E, Lass-Flörl C. 2014. Mucormycosis: from the pathogens to the disease. Clin Microbiol Infect 6:60–66. https://doi.org/10.1111/1469-0691.12566.
9. Lee SC, Li A, Calo S, Heitman J. 2013. Calcineurin plays key roles in the dimorphic transition and virulence of the human pathogenic zygomycete *Mucor circinelloides*. PLoS Pathog 9:e1003625. https://doi.org/10.1371/journal.ppat.1003625.
10. Patiño-Medina JA, Maldonado-Herrera G, Pérez-Arques C, Alejandre-Castañeda V, Reyes-Mares NY, Valle-Maldonado MI, Campos-García J, Ortiz-Alvarado R, Jácome-Galarza IE, Ramírez-Díaz MI, Garre V, Meza-Carmen V. 2018. Control of morphology and virulence by ADP-ribosylation factors (Arf) in *Mucor circinelloides*. Curr Genet 64:853–869. https://doi.org/10.1007/s00294-017-0798-0.
11. Patiño-Medina JA, Valle-Maldonado MI, Maldonado-Herrera G, Pérez-Arques C, Jácome-Galarza IE, Díaz-Pérez C, Díaz-Pérez AL, Araiza-Cervantes CA, Villagomez-Castro JC, Campos-García J, Ramírez-Díaz MI, Garre V, Meza-Carmen V. 2019. Role of Arf-like proteins (Arl1 and Arl2) of *Mucor circinelloides* in virulence and antifungal susceptibility. Fungal Genet Biol 129:40–51. https://doi.org/10.1016/j.fgb.2019.04.011.
12. Liu M, Spellberg B, Phan QT, Fu Y, Fu Y, Lee AS, Edwards JE, Jr, Filler SG, Ibrahim AS. 2010. The endothelial cell receptor GRP78 is required for mucormycosis pathogenesis in diabetic mice. J Clin Invest 120:1914–1924. https://doi.org/10.1172/JCI42164.
13. Patiño-Medina JA, Vargas-Tejeda D, Valle-Maldonado MI, Alejandre-Castañeda V, Jácome-Galarza IE, Villegas-Moreno J, Nuñez-Anita RE, Ramírez-Díaz MI, Ortiz-Alvarado R, Meza-Carmen V. 2019. Sporulation on blood serum increases the virulence of *Mucor circinelloides*. Microb Pathog 137:103737. https://doi.org/10.1016/j.micpath.2019.103737.
14. Brunke S, Mogavero S, Kasper L, Hube B. 2016. Virulence factors in fungal pathogens of man. Curr Opin Microbiol 32:89–95. https://doi.org/10.1016/j.mib.2016.05.010.
15. Ramage G, Mowat E, Jones B, Williams C, Lopez-Ribot J. 2009. Our current understanding of fungal biofilms. Crit Rev Microbiol 35:340–355. https://doi.org/10.3109/10408410903241436.
16. Mukherjee PK, Mohamed S, Chandra J, Kuhn D, Liu S, Antar OS, Munyon R, Mitchell AP, Andes D, Chance MR, Rouabhia M, Ghannoum MA. 2006. Alcohol dehydrogenase restricts the ability of the pathogen *Candida albicans* to form a biofilm on catheter surfaces through an ethanol-based mechanism. Infect Immun 74:3804–3816. https://doi.org/10.1128/IAI.00161-06.
17. Grahl N, Puttikamonkul S, Macdonald JM, Gamcsik MP, Ngo LY, Hohl TM, Cramer RA. 2011. *In vivo* hypoxia and a fungal alcohol dehydrogenase influence the pathogenesis of invasive pulmonary aspergillosis. PLoS Pathog 7:e1002145. https://doi.org/10.1371/journal.ppat.1002145.
18. Rangel-Porras RA, Meza-Carmen V, Martinez-Cadena G, Torres-Guzmán JC, González-Hernández GA, Arnau J, Gutiérrez-Corona JF. 2005. Molecular analysis of an NAD-dependent alcohol dehydrogenase from the zygomycete *Mucor circinelloides*. Mol Genet Genomics 274:354–363. https://doi.org/10.1007/s00438-005-0025-4.
19. Valle-Maldonado MI, Jácome-Galarza IE, Gutiérrez-Corona F, Ramírez-Díaz MI, Campos-García J, Meza-Carmen V. 2015. Selection of reference genes for quantitative real time RT-PCR during dimorphism in the zygomycete *Mucor circinelloides*. Mol Biol Rep 42:705–711. https://doi.org/10.1007/s11033-014-3818-x.
20. Rangel-Porras RA, Díaz-Pérez SP, Mendoza-Hernández JM, Romo-Rodríguez P, Alejandre-Castañeda V, Valle-Maldonado MI, Torres-Guzmán JC, González-Hernández GA, Campos-Garcia J, Arnaud J, Meza-Carmen V, Gutiérrez-Corona JF. 2019. Alcohol dehydrogenase 1 participates in the Crabtree effect and connects fermentative and oxidative metabolism in the Zygomycete *Mucor circinelloides*. J Microbiol 57:606–617. https://doi.org/10.1007/s12275-019-8680-z.
21. McIntyre M, Breum J, Arnau J, Nielsen J. 2002. Growth physiology and dimorphism of *Mucor circinelloides* (syn. *racemosus*) during submerged batch cultivation. Appl Microbiol Biotechnol 58:495–502. https://doi.org/10.1007/s00253-001-0916-1.
22. Li CH, Cervantes M, Springer DJ, Boekhout T, Ruiz-Vazquez RM, Torres-Martinez SR, Heitman J, Lee SC. 2011. Sporangiospore size dimorphism is linked to virulence of *Mucor circinelloides*. PLoS Pathog 7:e1002086. https://doi.org/10.1371/journal.ppat.1002086.
23. Sheppard DC, Filler SG. 2014. Host cell invasion by medically important fungi. Cold Spring Harb Perspect Med 5:a019687. https://doi.org/10.1101/cshperspect.a019687.
24. Karamanakos PN, Pappas P, Boumba VA, Thomas C, Malamas M, Vougiouklakis T, Marselos M. 2007. Pharmaceutical agents known to produce disulfiram-like reaction: effects on hepatic ethanol metabolism and brain monoamines. Int J Toxicol 26:423–432. https://doi.org/10.1080/10915810701583010.
25. Chayakulkeeree M, Ghannoum M, Perfect J. 2006. Zygomycosis: the reemerging fungal infection. Eur J Clin Microbiol Infect Dis 25:215–229. https://doi.org/10.1007/s10096-006-0107-1.
26. Ibrahim AS, Spellberg B. 2006. Zygomycetes as agents of infectious disease in humans, p 429–440. *In* Heitman J, Filler SG, Edwards JE, Jr, Mitchell AP (ed), Molecular principles of fungal pathogenesis. ASM Press, Washington, DC.
27. Neblett Fanfair R, Benedict K, Bos J, Bennett SD, Lo YC, Adebanjo T, Etienne K, Deak E, Derado G, Shieh WJ, Drew C, Zaki S, Sugerman D, Gade L, Thompson EH, Sutton DA, Engelthaler DM, Schupp JM, Brandt ME, Harris JR, Lockhart SR, Turabelidze G, Park BJ. 2012. Necrotizing cutaneous mucormycosis after a tornado in Joplin, Missouri. N Engl J Med 367:2214–2225. https://doi.org/10.1056/NEJMoa1204781.
28. Bartnicki-Garcia S. 1963. Symposium on biochemical bases of morphogenesis in fungi. III. Mold-yeast dimorphism of *Mucor*. Bacteriol Rev 27:293–304.
29. Sypherd PS, Borgia PT, Paznokas JL. 1978. Biochemistry of dimorphism in the fungus *Mucor*. Adv Microb Physiol 18:67–104. https://doi.org/10.1016/s0065-2911(08)60415-4.
30. Torres-Guzman JC, Arreola-Garcia GA, Zazueta-Sandoval R, Carrillo-Rayas T, Martinez-Cadena G, Gutierrez-Corona F. 1994. Genetic evidence for independence between fermentative metabolism (ethanol accumulation) and yeast-cell development in the dimorphic fungus *Mucor rouxii*. Curr Genet 26:166–171. https://doi.org/10.1007/bf00313806.
31. Wolff AM, Appel KF, Petersen JB, Poulsen U, Arnau J. 2002. Identification and analysis of genes involved in the control of dimorphism in *Mucor circinelloides* (syn. *racemosus*). FEMS Yeast Res 2:203–213. https://doi.org/10.1111/j.1567-1364.2002.tb00085.x.
32. Lübbehüsen T, González Polo V, Rossi S, Nielsen J, Moreno S, McIntyre M, Arnau J. 2004. Protein kinase A is involved in the control of morphology and branching during aerobic growth of *Mucor circinelloides*. Microbiology 150:143–150. https://doi.org/10.1099/mic.0.26708-0.
33. Ocampo J, Fernandez Nunez L, Silva F, Pereyra E, Moreno S, Garre V, Rossi S. 2009. A subunit of protein kinase A regulates growth and

differentiation in the fungus *Mucor circinelloides*. Eukaryot Cell 8:933–944. https://doi.org/10.1128/EC.00026-09.
34. Ocampo J, McCormack B, Navarro E, Moreno S, Garre V, Rossi S. 2012. Protein kinase A regulatory subunit isoforms regulate growth and differentiation in *Mucor circinelloides*: essential role of PKAR4. Eukaryot Cell 11:989–1002. https://doi.org/10.1128/EC.00017-12.
35. Aranda A, del Olmo M. 2003. Response to acetaldehyde stress in the yeast *Saccharomyces cerevisiae* involves a strain-dependent regulation of several ALD genes and is mediated by the general stress response pathway. Yeast 20:747–759. https://doi.org/10.1002/yea.991.
36. Seitz HK, Stickel F. 2010. Acetaldehyde as an underestimated risk factor for cancer development: role of genetics in ethanol metabolism. Genes Nutr 5:121–128. https://doi.org/10.1007/s12263-009-0154-1.
37. Nieminen MT, Novak-Frazer L, Rautemaa V, Rajendran R, Sorsa T, Ramage G, Bowyer P, Rautemaa R. 2014. A novel antifungal is active against *Candida albicans* biofilms and inhibits mutagenic acetaldehyde production in vitro. PLoS One 9:e97864. https://doi.org/10.1371/journal.pone.0097864.
38. Uittamo J, Siikala E, Kaihovaara P, Salaspuro M, Rautemaa R. 2009. Chronic candidosis and oral cancer in APECED-patients: production of carcinogenic acetaldehyde from glucose and ethanol by *Candida albicans*. Int J Cancer 124:754–756. https://doi.org/10.1002/ijc.23976.
39. Sapkota M, Wyatt TA. 2015. Alcohol, aldehydes, adducts and airways. Biomolecules 5:2987–3008. https://doi.org/10.3390/biom5042987.
40. Setshedi M, Wands JR, Monte SM. 2010. Acetaldehyde adducts in alcoholic liver disease. Oxid Med Cell Longev 3:178–185. https://doi.org/10.4161/oxim.3.3.12288.
41. Schopf RE, Trompeter M, Bork K, Morsches B. 1985. Effects of ethanol and acetaldehyde on phagocytic functions. Arch Dermatol Res 277:131–137. https://doi.org/10.1007/bf00414111.
42. Wolpe SD, Cerami A. 1989. Macrophage inflammatory proteins 1 and 2: members of a novel superfamily of cytokines. FASEB J 3:2565–2573. https://doi.org/10.1096/fasebj.3.14.2687068.
43. Henao-Mejia J, Elinav E, Strowig T, Flavell RA. 2012. Inflammasomes: far beyond inflammation. Nat Immunol 13:321–324. https://doi.org/10.1038/ni.2257.
44. Antachopoulos C, Roilides E. 2005. Cytokines and fungal infections. Br J Haematol 129:583–596. https://doi.org/10.1111/j.1365-2141.2005.05498.x.
45. Müller M, Mentel M, van Hellemond JJ, Henze K, Woehle C, Gould SB, Yu R-Y, van der Giezen M, Tielens AGM, Martin WF. 2012. Biochemistry and evolution of anaerobic energy metabolism in eukaryotes. Microbiol Mol Biol Rev 76:444–495. https://doi.org/10.1128/MMBR.05024-11.
46. Roncero MIG, Jepsen LP, Strøman P, van Heeswijck R. 1989. Characterization of a *leuA* gene and an *ARS* element from *Mucor circinelloides*. Gene 84:335–343. https://doi.org/10.1016/0378-1119(89)90508-8.
47. Salcedo-Hernández R, Ruiz-Herrera J. 1993. Isolation and characterization of a mycelial cytochrome aa_3-deficient mutant and the role of mitochondria in dimorphism of *Mucor rouxii*. Exp Mycol 17:142–154. https://doi.org/10.1006/emyc.1993.1013.
48. Pfaffl MW. 2001. A new mathematical model for relative quantification in real-time RT-PCR. Nucleic Acids Res 29:e45. https://doi.org/10.1093/nar/29.9.e45.
49. Brenner S. 1974. The genetics of *Caenorhabditis elegans*. Genetics 77:71–94.
50. Stiernagle T. 2006. Maintenance of *C. elegans*. Worm Book 11:1–11. https://doi.org/10.1895/wormbook.1.101.1.
51. Secretaría de Agricultura, Ganadería, Desarrollo Rural, Pesca y Alimentación (SAGARPA) NORMA Oficial Mexicana NOM-062-ZOO-1999. 2001. Especificaciones técnicas para la producción, cuidado y uso de los animales de laboratorio. Diario Oficial de la Federación 2:107–167. (In Spanish.)